# NEW CONVERGENCE CRITERIA FOR THE VORTEX-LATTICE MODELS OF THE LEADING-EDGE SEPARATION*

Osama A. Kandil, Dean T. Mook, and Ali H. Nayfeh
Virginia Polytechnic Institute and State University

## SUMMARY

The convergence criterion for the vortex-lattice technique which deals with delta wings exhibiting significant leading-edge separation has two requirements. First, the wake must converge to a force-free position for any given number of discrete vortex elements. Second, the distributed loads must converge as the number of elements increases. Replacing the vortex sheets representing the wakes by a system of discrete vortex lines whose positions are determined as part of the solution (first requirement), one finds that the total loads computed agree very well with experimental data. But the predicted pressure distributions have some irregularities which are the result of discrete vortex lines coming close to the lifting surface. Here it is shown that one can eliminate these irregularities and predict pressure distributions which agree fairly well with experimental data (which show some irregularities of their own) by replacing the system of discrete vortex lines with a single concentrated core. This core has a circulation equal to the algebraic sum of the circulations around the discrete lines and is located at the centroid of these lines. Moreover, the second requirement is replaced by the requirement that the position and strength of the core converge as the number of elements increases. Because the calculation of the position and strength of the core is much less involved than the calculation of the loads, this approach has the additional desirable feature of requiring less computational time.

16

## INTRODUCTION

A characteristic feature of the flow over wings having highly swept, sharp leading edges is the formation of vortices above suction sides in the vicinity of the leading edges. These vortices roll up in a conical-like spiral with a concentrated core. This vortex spiral grows in size and strength as it approaches

*This work was supported by the NASA Langley Research Center under Grant No. NSG 1262.

the trailing edge. Below the angle of stall (i.e., the angle at which vortex bursting occurs), the effect of the leading-edge separation is to increase the velocity on the suction side of the lifting surface by adding a strong cross-flow component and hence to increase the aerodynamic loads. Experimental investigations, such as those described in refs. 1-7, and numerical investigations, such as those described in refs. 8 and 9, confirm these conclusions. Detailed descriptions of the flow field are also given in these references.

Though the experimental results show that the pressure distribution is somewhat influenced by the character (laminar or turbulent) of the boundary layer, the lift and pitching-moment coefficients are independent of the Reynolds number. Thus, one expects an inviscid model of the flow to predict the total loads more reliably than the distributed loads. And such has turned out to be the case.

The early attempts to develop an inviscid model of these flows were based on assumptions of conical flow and/or slender-body theory. These assumptions are apparently discredited by the experimental observations; more discussion is given in references 8 and 9.

Subsequent attempts to develop inviscid models did not use these assumptions. Rehbach (ref. 10) developed a vortex-lattice technique which progressively shortens the leading edge of a rectangular wing until a delta wing is formed. Associated with this method are questions concerning the second convergence requirement and the undesirable feature of long computation times; more discussion is given in refs. 8 and 9. Weber et al (ref. 11) developed a technique which uses piecewise continuous, quadratic, doublet-sheet distributions. The second requirement apparently was not considered, and no results showing the computed shapes of the rolled-up wakes were given.

In a related effort, Suciu and Morino (ref. 12) developed a technique for modelling the region adjoining the trailing edge. However, numerical experiments, as described in refs. 8 and 9, show that the wake adjoining the trailing edge has very little influence on the aerodynamic loads.

In the present paper, the question of the convergence of the centroidal line as the number of discrete elements increases is considered; and this line, instead of the system of discrete vortex lines, is used to compute the pressure.

## SYMBOLS

| | |
|---|---|
| AR | aspect ratio |
| b | wing semi-span |
| $C_{mz}$ | pitching-moment coefficient about the z-axis |
| $C_n$ | normal-force coefficient |
| $c_n(x)$ | local cross-normal-force coefficient |
| $\Delta C_p$ | pressure coefficient |
| $c_r$ | root chord |
| s(x)/b | local semi-span/wing semi-span |
| $t/c_r$ | thickness ratio |
| $\bar{U}_\infty$ | free-stream velocity |
| x,y,z | body-fixed axes (z-axis is in spanwise direction) |
| $x/c_r$ | dimensionless chord station |
| z/s(x) | dimensionless spanwise station |
| $\alpha$ | angle of attack |
| $\Gamma/c_r U_\infty$ | dimensionless circulation |
| nel | number of elemental areas of the lattice |

## FORMULATION OF THE PROBLEM

The perturbation velocity potential, $\phi$, of the inviscid, irrotational, incompressible flow past a wing is governed by Laplace's equation and satisfies the following boundary conditions: (a) the no-penetration condition on the wing surface given by

$$(\bar{U}_\infty + \nabla\phi) \cdot \bar{n} = 0 \quad \text{on } S(\bar{r}) = 0$$

where $\bar{n}$ is the unit normal to the wing surface S, (b) the no-pressure discontinuity condition across the wakes emanating from the leading and trailing edges of the wing given by

$$\Delta p = 0 \quad \text{across } w(\bar{r}) = 0$$

where $\Delta p$ is the pressure jump across the wake surface w. This surface is an unknown of the problem and must be obtained as part of the solution, (c) the Kutta condition which requires that no-pressure jump exists across the wing surface along the leading and trailing edges where the wake surface is emanating, and (d) the disturbance velocity, $\nabla\phi$, diminishes far from the wing surface, S, and the wake surface, w. We note that the problem is nonlinear due to boundary condition (b).

## DESCRIPTION OF THE METHOD OF SOLUTION

The solution of the problem posed above is constructed by modelling the lifting surface with a bound-vortex lattice and the wake with a system of discrete, nonintersecting vortex lines. Each vortex line in the wake is composed of a series of short, straight segments and one final semi-infinite segment. The unknowns here are the circulations around the vortex segments and the positions of the finite segments in the wake.

The disturbance velocity field produced by this model of the wing and wake is calculated according to the Biot-Savart law; thus, everywhere, except on the wing and the wake, Laplace's equation is satisfied. Moreover, the disturbance created by the wing dies out far from the wing and wake, boundary condition (d).

Associated with each elemental area of the lattice and with each finite segment in the wake is a control point. The lattice is arranged so that vortex segments leaving the sharp edges do so at right angles to the edge. Moreover, control points are placed between the last edgewise vortex segment of each row and column and the edge itself. This arrangement partially satisfies the Kutta condition (c).

The circulations and the positions of the finite segments in the wake are obtained by simultaneously requiring the normal component of velocity to vanish at the control points of the elemental areas of the lattice and the finite segments in the wake to be parallel to the velocities at their own control points. Boundary conditions (a) and (b) and the Kutta condition (c) are then satisfied, and the problem is solved for this lattice (i.e., the first requirement of the convergence criterion is met). More details, especially those regarding the iterative procedure used to effect the last step, are given in refs. 8 and 9.

Instead of calculating the aerodynamic loads and testing the second requirement of convergence at this point, with the present procedure we calculate the centroidal line of the system of free-vortex lines representing the leading-edge wake. To construct this centroidal line, we consider a series of cross-flow planes. Proceeding from the vertex toward the trailing edge, we calculate the centroids of the vortex lines penetrating these planes according to

$$\vec{r}_j = \frac{\sum_{i=1}^{n_j} \Gamma_i \vec{r}_{ij}}{\Gamma_{cj}}$$

where $\Gamma_{cj}$ is taken to be the circulation around the centroidal line between the $j^{th}$ and $(j+1)^{th}$ planes and it given by

$$\Gamma_{cj} = \sum_{i=1}^{n_j} \Gamma_i$$

$\vec{r}_j$ is the position of the centroid in the $j^{th}$ plane, $\vec{r}_{ij}$ is the position of the intersection of the $i^{th}$ vortex line with the $j^{th}$ plane, $\Gamma_i$ is the circulation around the $i^{th}$ line, and $n_j$ is the number of lines penetrating the $j^{th}$ plane. More lines penetrate the planes near the trailing edge than those near the vertex; thus, $\Gamma_{cj}$ increases toward the trailing edge.

Now, the number of elements is increased and new centroidal lines are calculated until the changes in $\Gamma_{cj}$ and $\vec{r}_j$ fall within prescribed tolerances. At this point, the second requirement of the convergence criterion is met.

Only when both requirements are met, do we calculate the aerodynamic loads and pressure distribution. The details for calculating the loads are given in ref. 8. The numerical results below show, for the examples being considered at least, that the centroidal lines converge to a position which is very close to the experimentally determined position of the core, that the total loads agree very well with the experimental data, and that the pressure distributions agree fairly well with the experimental data.

## NUMERICAL EXAMPLES

Figures 1 and 2 show the actual calculated positions of the free-vortex lines for two delta wings. The plan view also shows the bound-vortex lattice. And the three dimensional view shows the free-vortex lines, their centroidal line, and the trace of the spiral vortex sheet. All the following results are associated with these two wings.

Figures 3 and 4 show the convergence of the circulations around the centroidal line. And figures 5-8 show the convergence of the position of the centroidal line and the close agreement between the position of the calculated line and the experimentally determined position of the vortex core.

Figures 9 and 10 show the convergence of the total loads calculated by using the system of discrete lines and by using the centroidal line as a function of the number of elements (nel). These results are compared with those obtained by the leading-edge-suction analogy (ref. 13) and with experimental data. We note

that there is a considerable difference in the experimentally determined normal-force coefficients in figure 10.

Figures 11 and 12 show comparisons of the predicted cross-load coefficients and experimental data. And figures 13-16 show comparisons of the predicted pressure distributions at several chordwise stations with those obtained by another method (ref. 11) and with experimental data. We note that the shape and size of the suction peak on the upper surface under the vortex differ from one experiment to another, depending on how thick the wing is and on whether the boundary layer is laminar or turbulent (refs. 5, 6, and 14).

## CONCLUDING REMARKS

The second requirement of convergence is based on the centroidal line of the free-vortex lines representing the wake. Using this requirement greatly reduces the computational time. The position of the centroidal line compares very well with that of the vortex core. The centroidal line can also be used to calculate the total and distributed aerodynamic loads with good accuracy. This results in more reduction in the computational time and smoothing of the peaks produced by using many discrete lines.

## REFERENCES


1. Peckham, D. H., "Low-Speed Wind-Tunnel Tests on a Series of Uncambered Slender Pointed Wings with Sharp Edges", R & M No. 3186, Brit. ARC, 1961.
2. Bergesen, A. J., and Porter, J. D., "An Investigation of the Flow Around Slender Delta Wings with Leading-Edge Separation", Princeton University, Department of Aeronautical Engineering, Report No. 510, May 1960.
3. Nangia, R. K., and Hancock, G. J., "Delta Wings with Longitudinal Camber at Low Speed", C.P. No. 1129, Brit. ARC, 1970.
4. Marsden, D. J., Simpson, R. W., and Rainbird, B. E., "An Investigation into the Flow over Delta Wings at Low Speeds with Leading-Edge Separation", The College of Aeronautics, Cranfield, Report No. 114, February 1958.
5. Hummel, D., "Study of the Flow Around Sharp-Edged Slender Delta Wings with Large Angles of Attack", NASA TT F-15,107, September 1973.
6. Hummel, D. and Redeker, G., "Experimental Determination of Bound Vortex Lines and Flow in the Vicinity of the Trailing Edge of a Slender Delta Wing", NASA TT F-15,012, August 1973.
7. Bartlett, G. E., and Vidal, R. K., "Experimental Investigation of Influence of Edge Shape on the Aerodynamic Characteristics of Low-Aspect-Ratio Wings at Low Speeds", Journal of Aeronautical Sciences, Vol. 22, No. 8, August 1955, pp. 517-533.
8. Kandil, O. A., "Prediction of the Steady Aerodynamic Loads on Lifting Surfaces having Sharp-Edge Separation", Ph.D. Dissertation, Engineering Science and Mechanics Department, Virginia Polytechnic Institute and State University, December 1974.
9. Kandil, O. A., Mook, D. T., and Nayfeh, A. H., "Nonlinear Prediction of the Aerodynamic Loads on Lifting Surfaces. AIAA Paper No. 74-503, June 1974. Also in Journal of Aircraft, Vol. 13, No. 1, January 1976, pp. 22-28.
10. Renbach, C., "Numerical Investigation of Vortex Sheets Issuing from Separation Line near the Leading Edge", NASA TT F-15, 530, 1974.
11. Weber, J. A., Brune, G. W., Johnson, F. T., Lu, P., and Rubbert, P. E., "A Three-Dimensional Solution of Flows Over Wings with Leading-Edge-Vortex Separation", NASA SP-347, Part II, 1975, pp. 1013-1032.

12. Suciu, E. O., and Morino, L., "A Nonlinear Finite-Element Analysis of Wings in Steady Incompressible Flows with Wake Roll-Up", AIAA Paper No. 76-64, January 1976.

13. Polhamus, E. C., "A Concept of the Vortex Lift of Sharp-Edge Delta Wings Based on a Leading-Edge-Suction Analogy", NASA TN D-3767, December 1966.

14. Smith, J. H. B., "Improved Calculations of Leading-Edge Separation from Slender, Thin, Delta Wings", Proc. Roy. Soc. A. 306, 1968, pp. 67-90.

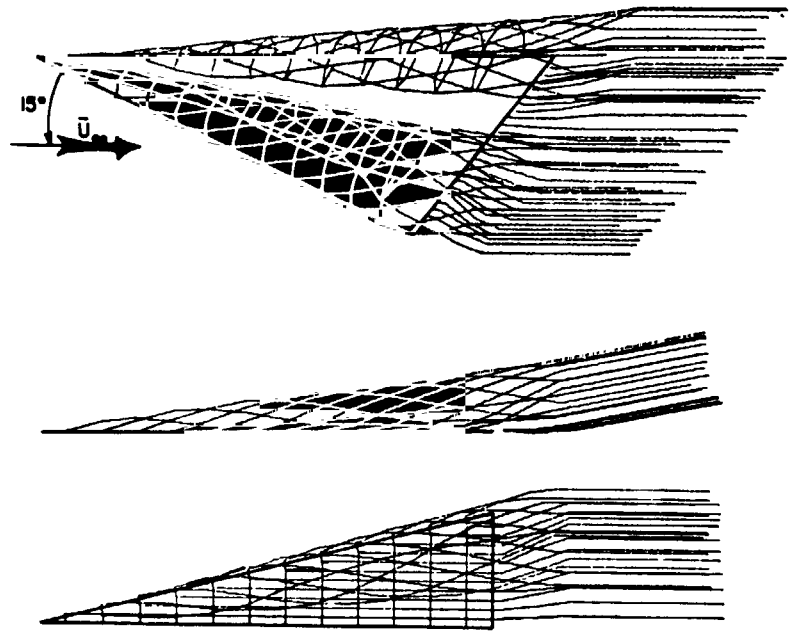


Figure 1.- A typical solution of the wake shape for a delta wing with $\mathcal{R}$ = 1. 12×12 lattice.

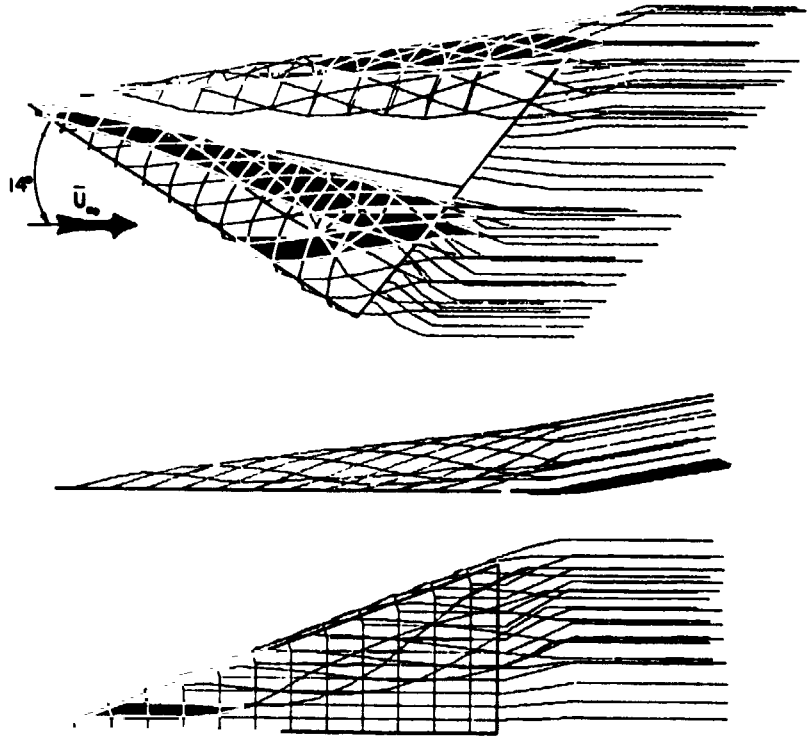


Figure 2.- A typical solution of the wake shape for a delta wing with $\mathcal{R}$ = 1.46. 12×12 lattice.

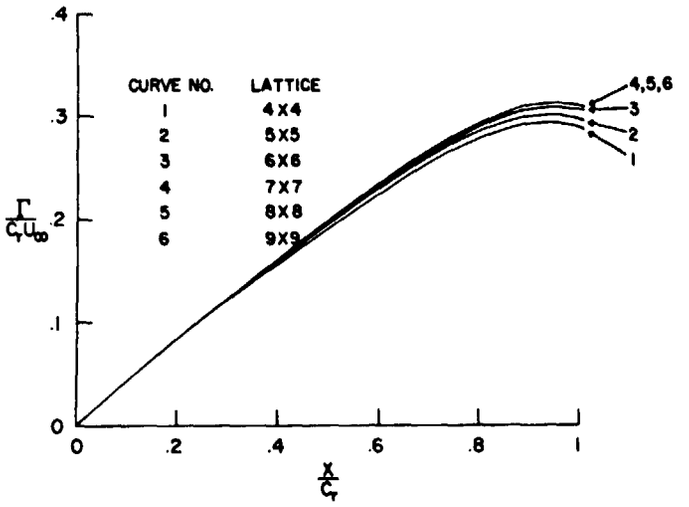


Figure 3.- Variation of circulation along the vortex core of a delta wing with $A_R = 1$. $\alpha = 15^\circ$.

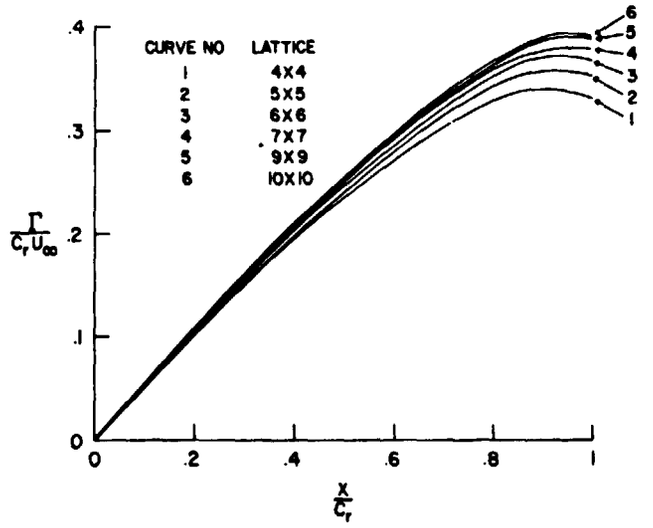


Figure 4.- Variation of circulation along the vortex core of a delta wing with $A_R = 1.46$. $\alpha = 14^\circ$.

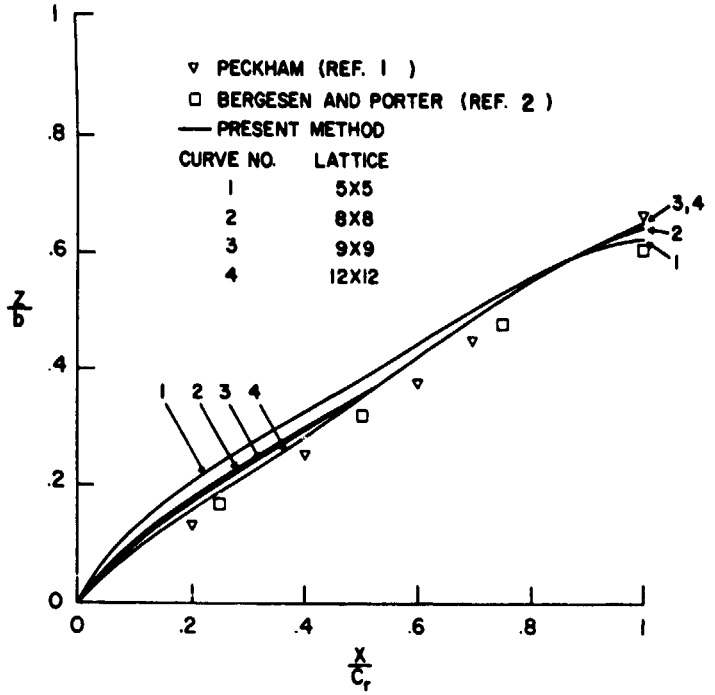


Figure 5.- Spanwise position of vortex-core path on a delta wing with $\mathcal{R} = 1$. $\alpha = 15^{\circ}$.

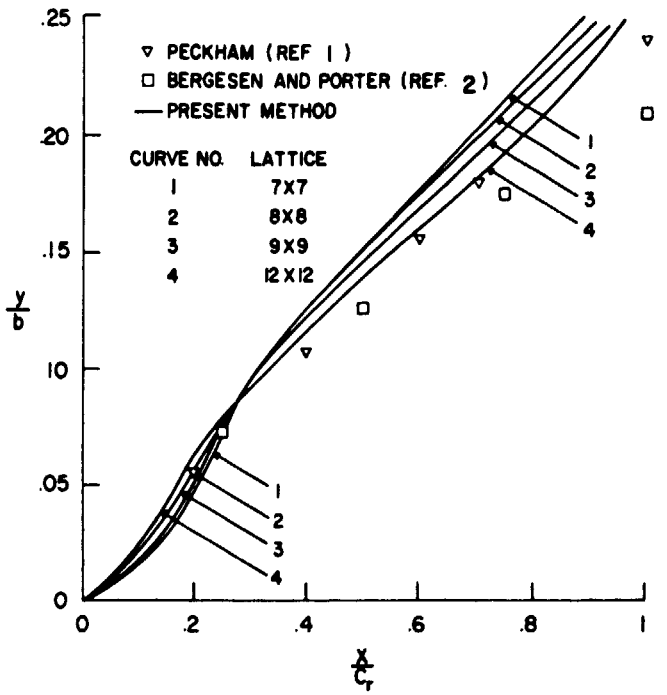


Figure 6.- Height of vortex-core path on a delta wing with $\mathcal{R} = 1$. $\alpha = 15^{\circ}$.

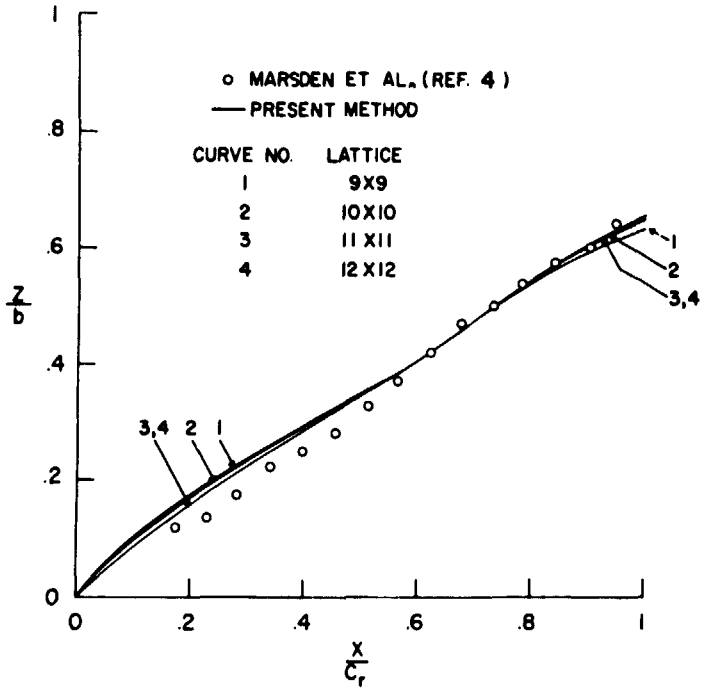


Figure 7.- Spanwise position of vortex-core path on a delta wing with $\mathcal{R} = 1.46$. $\alpha = 14^{\circ}$.

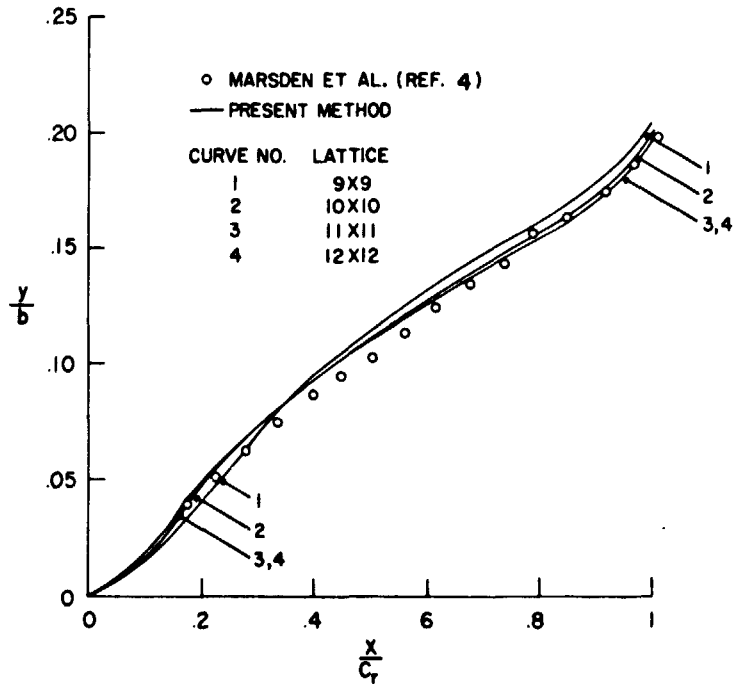


Figure 8.- Height of vortex-core path on a delta wing with $\mathcal{R} = 1.46$. $\alpha = 14^{\circ}$.

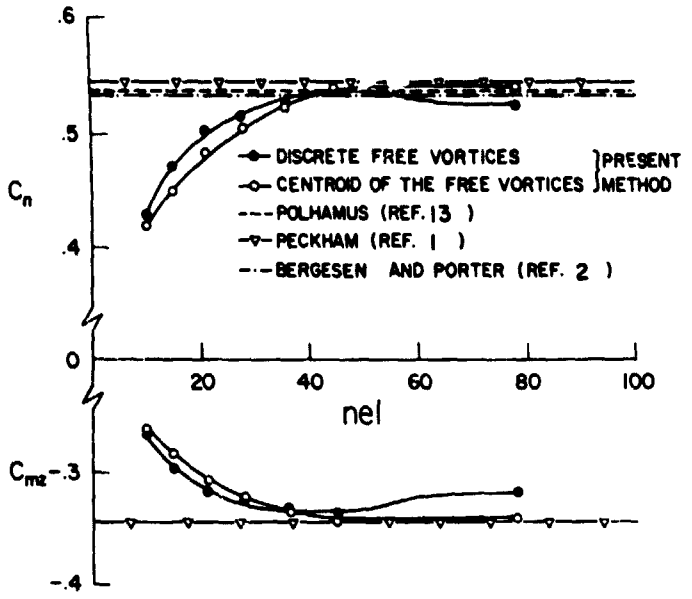


Figure 9.- Normal-force and pitching-moment coefficients of a delta wing with $AR = 1$. $\alpha = 15^{\circ}$.

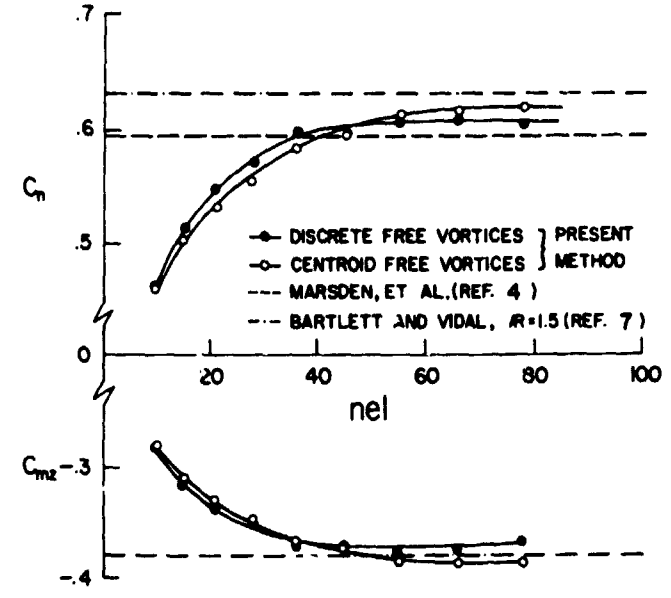


Figure 10.- Normal-force and pitching-moment coefficients of a delta wing with $AR = 1.46$. $\alpha = 14^{\circ}$.

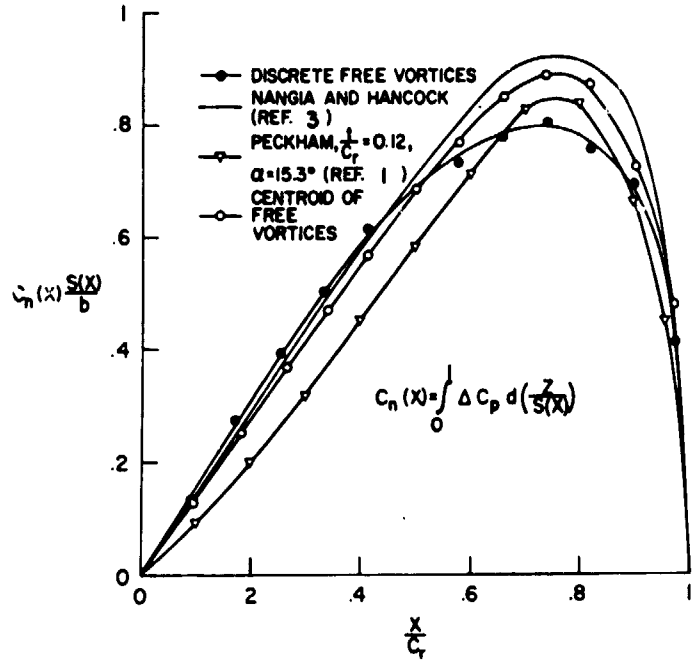


Figure 11.- Longitudinal distribution of cross load for a delta wing with AR = 1. 12×12 lattice; $\alpha = 15^{o}$.

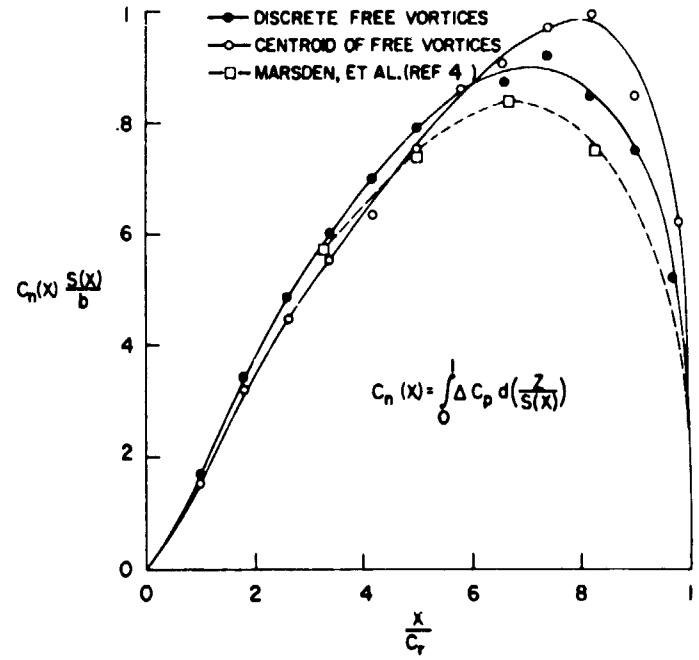


Figure 12.- Longitudinal distribution of cross load for a delta wing with AR = 1.46. 12×12 lattice; $\alpha = 14^{o}$.

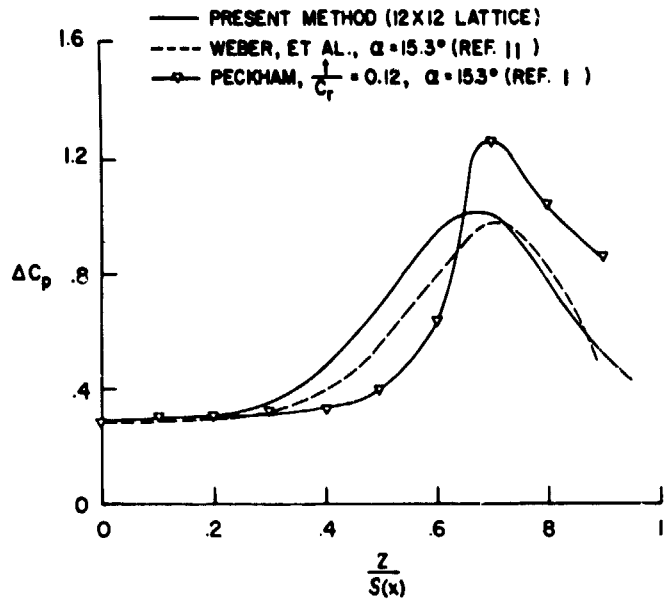


Figure 13.- Surface pressure distribution of a delta wing at $\frac{x}{c_r} = 0.7$. $AR = 1$; $\alpha = 15^{o}$.

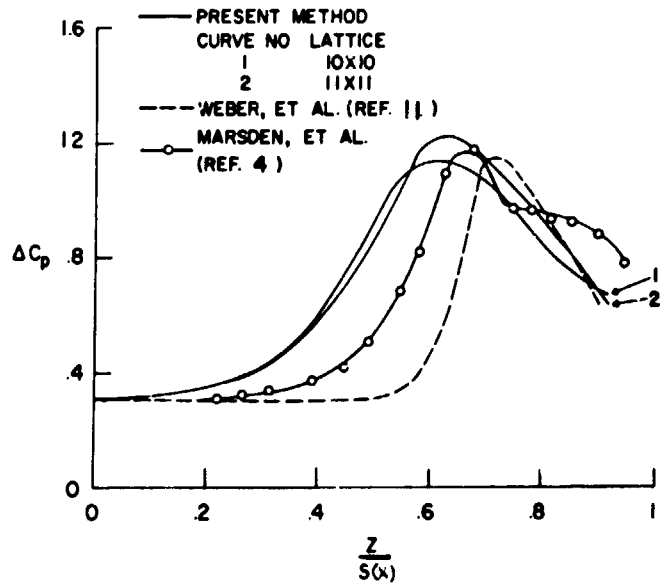


Figure 14.- Surface pressure distribution of a delta wing at $\frac{x}{c_r} = 0.82$. $AR = 1$; $\alpha = 15^{o}$.

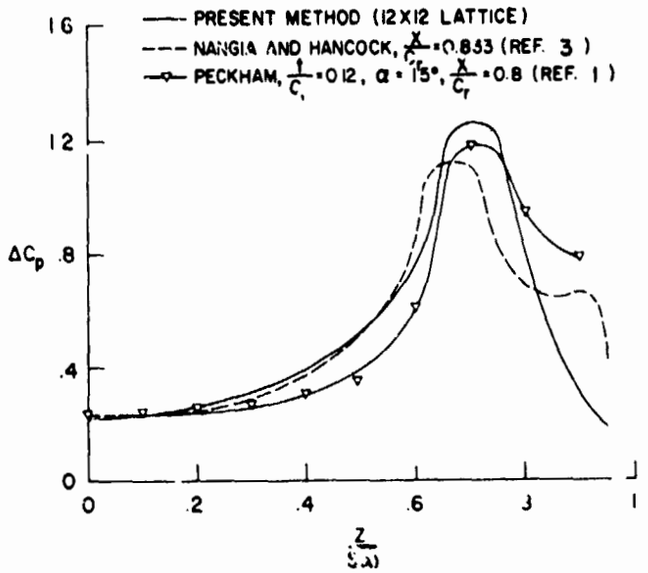


Figure 15.- Surface pressure distribution of a delta wing at $\frac{x}{c_r}$ = 0.67. AR = 1.46; $\alpha = 14^{o}$.

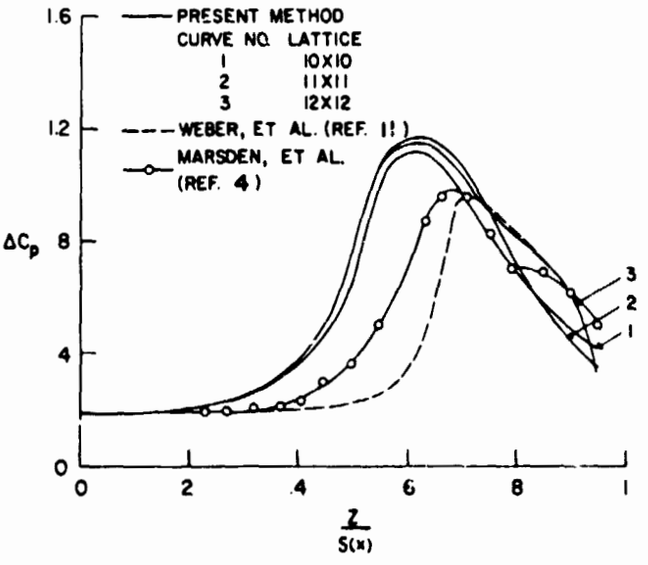


Figure 16.- Surface pressure distribution of a delta wing at $\frac{x}{c_r}$ = 0.83. AR = 1.46; $\alpha = 14^{o}$.